Design and Performance Analysis of Magnetic Bearings for Vehicle High-speed Flywheel Battery

Di Huang, Binbin Sun, Tianqi Gu, Zhenwei Wang, Tiezhu Zhang and Yang Wang

Abstract—**Flywheel batteries have been widely used in the aerospace and transportation fields due to their advantages of high power, fast response, and high efficiency. Among them, the magnetic levitation bearing is the key to realize the high-speed and high-efficiency operation of flywheel batteries. In this paper, the research object is the flywheel battery for automotive applications. First, the third-order critical mode characteristics of the flywheel battery are analyzed and the topology scheme of the flywheel battery support structure is designed. Then, the radial magnetic levitation bearing rotor and stator are designed, and the axial magnetic levitation bearing stator and thrust disk are designed. The closed-loop differential control strategy of the magnetic bearing is designed. The system control transfer function is derived. Finally, the strength of magnetic induction in the axial magnetic bearing is verified. The influence of the excitation mode of the radial magnetic bearing on the magnetic circuit distribution and magnetic pole coupling is analyzed, and the NNSS type topology scheme is determined. The dynamic response characteristics of the bearing system are analyzed, and the designed magnetic levitation bearing can levitate the flywheel rotor according to the operational requirements when influenced by external steps and sinusoidal excitation.**

Index Terms—**flywheel battery, magnetic levitation bearing, modal analysis, structural design**

I. Introduction

FLYWHEEL battery, as a physical energy storage method, compared with traditional chemical batteries, has many advantages such as high energy conversion efficiency, high instantaneous power, fast response speed, long service life, low environmental impact and so on, which is a promising short-time high-power energy storage technology with great development and market potential [1,2]. It can be applied in many fields, such as high-quality uninterruptible power supply (UPS), pulse power supply, grid frequency regulation, and renewable energy grid connection[3]. If the flywheel battery is applied to vehicles, it can realize the recovery, storage and reuse of vehicle braking energy, and play the role of "peak shaving and valley filling". It can also make the vehicle more advantageous in starting, accelerating, and braking energy recovery [4,5].

For high power density, high energy density flywheel battery, due to the high mass of the flywheel rotor and high rotational inertia, its gyroscopic effect at high speed is obvious and there is the problem of over-critical speed [6]. Li proposed a novel electromagnetically coupled flywheel energy storage system to enhance the performance of front-drive electric vehicles [7]. Nevertheless, the support of the flywheel rotor in the system is designed based on mechanical bearings and only meets the requirements of low-speed conditions. Traditional mechanical bearings, such as deep groove ball bearings and angular contact bearings, are in direct contact with the rotating shaft during operation. Especially in the case of the high rotational speed of flywheel rotor, such as tens of thousands of rotational speed, the safety of the system is seriously affected by the high-temperature rise of the rotor shaft and bearings owing to excessive friction. It is not only hard to meet the support requirements of the flywheel rotor but also has excessive losses, and is unable to meet the technical specifications of high-speed fly-wheel batteries [8]. Therefore, as one of the key technologies of flywheel batteries, bearing technology that can adapt to high speed and low loss requirements is directly related to the efficiency and lifespan of flywheel batteries [9]. Consequently, high-performance, high-speed magnetic bearings are applied to the novel high-speed flywheel battery system.

Compared to conventional contact mechanical bearings, magnetic levitation bearings are widely used in high-speed flywheel cell systems due to their advantages such as low noise, energy efficiency, no wear, and controllable stiffness and damping [10]. Nevertheless, applying the support scheme for flywheel battery systems based on mechanical bearing design directly to the novel magnetic levitation bearing-based high-speed flywheel battery system is

Manuscript received March 15, 2023; revised September 20, 2023.

This work was supported in part by the Innovation team project of "Qing-Chuang science and technology plan" of colleges and universities in Shandong Province 2021KJ083, the key R & D projects in Shandong under Grant 2019GHZ016， the Major Innovation Projects in Shandong under Grant 2020CXGC010405 and 2020CXGC010406, the Postdoctoral Science Foundation of China and Shandong under Grant 2020M680091.

Di Huang is a graduate student of School of Transportation and Vehicle Engineering, Shandong University of Technology, Zibo, 255000 PR China. (e-mail: huangdi934675559@163.com).

Binbin Sun is a Professor of School of Transportation and Vehicle Engineering, Shandong University of Technology, Zibo, 255000 PR China. (corresponding author to provide phone: 86-13708941464; e-mail: sunbin_sdut@126.com).

Tianqi Gu is a graduate student of School of Transportation and Vehicle Engineering, Shandong University of Technology, Zibo, 255000 PR China. (e-mail: tianqi.gu@outlook.com).

Zhenwei Wang is a graduate of School of Transportation and Vehicle Engineering, Shandong University of Technology, Zibo, 255000 PR China. (e-mail: zhenweiwang2022@163.com).

Tiezhu Zhang is a Professor of School of Transportation and Vehicle Engineering, Shandong University of Technology, Zibo, 255000 PR China. (e-mail: qdzhangtz@163.com).

Yang Wang is a graduate student of School of Transportation and Vehicle Engineering, Shandong University of Technology, Zibo, 255000 PR China. (e-mail: goodluck4wy@163.com).

challenging [11]. Consequently, scholars conducted further studies in the areas of support scheme design, optimization of magnetic bearing structures, and design of magnetic bearing control systems [12].

Magnetic levitation bearings can be generally classified into three types: active magnetic levitation bearings, passive magnetic levitation bearings, and hybrid magnetic levitation bearings [13]. Among them, active magnetic levitation bearings are the most widely used magnetic levitation bearings, whose stiffness and damping can be adjusted by the controller to better achieve the goal of stable rotor levitation [14]. Nikolaj designed a novel support solution for flywheel energy storage systems based on active magnetic bearings. Its axial load is provided by permanent magnets and active magnetic bearings are provided for radial stabilization. The feasibility of the design approach was verified by numerical and experimental results [15]. Nevertheless, increasing load carrying capacity, reducing loss, and minimizing size have become the current research priorities for high-performance maglev bearings. Additionally, radial maglev bearings of the conventional structure have the problem of local magnetic force line clustering, which needs to be further optimized [16].

With the continuous research conducted by researchers on active magnetic levitation bearings for their application in flywheel energy storage systems, their is a need to address the requirements for their high-quality operation [17]. Tukesh Soni studied the performance of electromagnetic bearings for flywheel energy storage systems and the results showed that the electromagnetic bearings require additional design and control corrections to ensure operation under complex conditions [18]. Consequently, convenient controls are continuously studied to achieve the high-quality performance of electromagnetic bearings [19]. In particular, PID control and sliding mode control are continuously applied to the high response of electromagnetic bearings control [20-22]. However, for active magnetic bearings, which are oriented to vehicle applications, there are still problems such as bearing modal characteristics analysis, support structure topology scheme design, and radial and axial magnetic bearing electromagnetic field design.

In this paper, a novel magnetic bearing for vehicle high-speed flywheel battery is studied. The research is carried out by the design of the novel support structure topology scheme, the design of the novel active magnetic levitation bearing, and the building of the control system. The main contributions are summarized as follows. (1) The active magnetic levitation bearing is applied to the flywheel battery, and the innovative design provides a novel solution for the design of a class of novel flywheel battery support schemes. (2) A scheme for optimizing the structure of a radial magnetic levitation bearing is designed to enhance the load-bearing capacity and effectively reduce the edge effect and clustering of magnetic lines of force at the magnetic pole. (3) The feasibility of the designed prototype and the scheme is verified by simulation and test results.

The rest of the work is scheduled as follows. In Section 2, a novel support structure topology scheme is designed based on the modal analysis of the flywheel cell. In sections 3 and 4, the structures of radial electromagnetic bearing and axial electromagnetic bearing are designed. In Section 5, the control system for the active magnetic levitation bearing is built. In Section 6, the performance of the system is analyzed and verified in experiments. In Section 7, the entire paper is summarized.

II. Flywheel Battery Support Structure Topology Design

A. Modal analysis of the flywheel rotor

According to the design requirement of the flywheel battery, the maximum rotor speed is 45000 r/min. The operating speed range of the rotor is 14,000~45,000 r/min [23]. To guide the layout design of the maglev bearing and the design of the controller, modal analysis is carried out.

Since the fourth-order critical speed of the flywheel rotor exceeds its maximum design speed, this paper mainly studies the vibration mode characteristics of the first-order, second-order, and third-order critical speed boundary of the flywheel rotor. The maximum speed modal of the flywheel cell rotor is shown in Fig. 1(a). As shown in Fig. 1(b), the first-order critical speed of the flywheel cell rotor is 2808.7 r/min, and the flywheel rotor exhibits flat motion and is subjected to less shock. As shown in Fig. 1(c), the second-order critical speed of the flywheel cell rotor is 17035.8 r/min, and the flywheel rotor oscillates. The impact is intensified, and the gyroscopic effect phenomenon appears. As shown in Fig. 1(d), the third-order critical speed of the fly-wheel cell rotor is 17415.6 r/min, and the oscillation of the flywheel rotor is more obvious and the gyroscopic effect is intense under the speed.

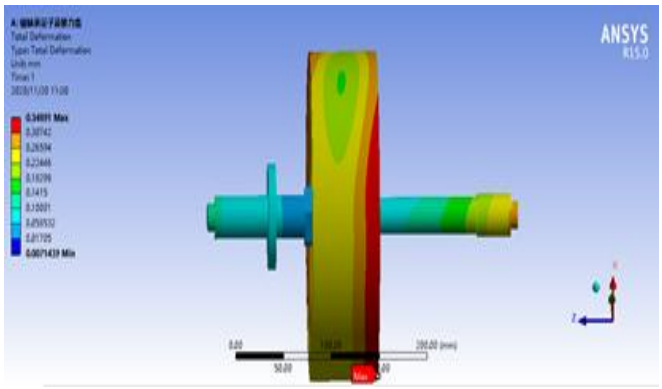

(a) Maximum speed modal

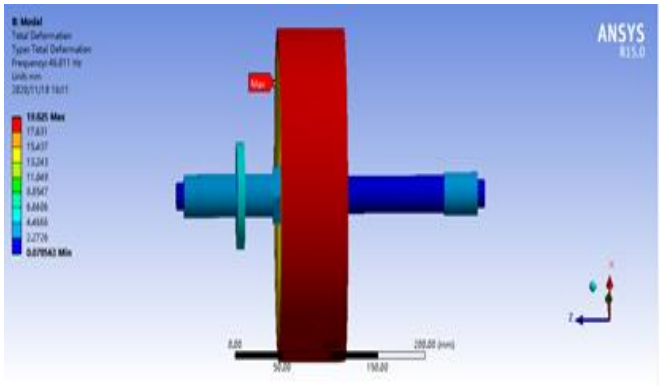

(b) First-order modal

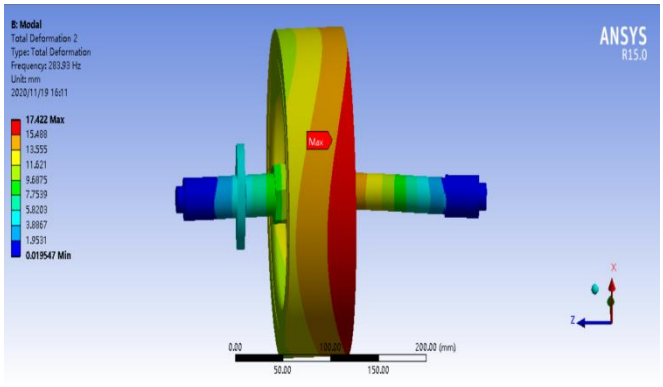

(c) Second-order modal

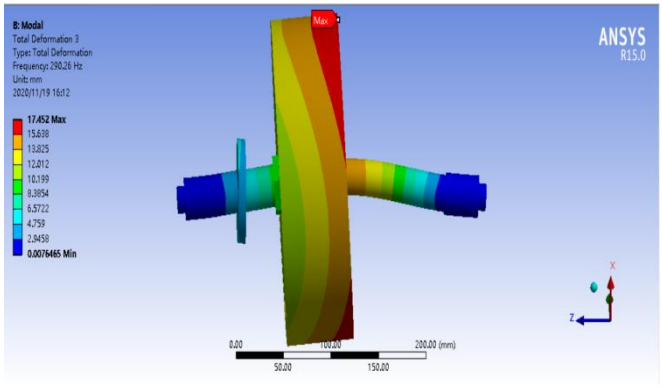

(d) Third-order modal

Fig. 1 Flywheel rotor critical speed vibration type

In summary, the acceleration process of the flywheel cell rotor undergoes a gradual transition from linear motion to oscillation, and then from oscillation to bending. As rotor speed of the flywheel approaches the critical speed, the maglev bearing needs to increase the bias current accordingly in order to enhance the stiffness of the maglev bearing. This ensures that the flywheel rotor smoothly crosses the critical speed. As the flywheel rotor speed approaches critical speed, the maglev bearing needs to increase the corresponding bias current to improve the stiffness of the maglev bearing. This ensures that the flywheel rotor crosses the critical speed smoothly.

B. Support structure topology scheme design

The flywheel rotor modal characteristics indicate that the flywheel cell rotor undergoes a change from flat motion to oscillation and then from oscillation to bending during the acceleration process. When designing the support structure topology, it is necessary to ensure that the flywheel rotor smoothly transitions through the critical speed point. To this end, a flywheel cell support structure topology scheme is designed as shown in Fig. 2, which includes two sets of radial magnetic levitation bearings, one set of axial magnetic levitation bearings, and two mechanical bearings at both ends. Among them, the mechanical bearings are auxiliary bearings, which play the role of protecting the magnetic levitation bearings. The two sets of radial magnetic levitation bearings are located on both sides of the flywheel rotor and motor rotor to limit the radial dis-placement of the flywheel cell spindle. The axial magnetic levitation bearings play the role of limiting the axial displacement of the flywheel cell main shaft. With the combined effect of the three sets of magnetic levitation bearings, the displacement of the flywheel cell spindle is controlled in five degrees of freedom.

When the flywheel cell is in non-operating condition, the auxiliary bearings pro-vide support for the flywheel cell spindle to balance the gravity of the flywheel cell system and maintain stability. When the flywheel cell is in normal operation, the fly-wheel cell spindle is free from the auxiliary bearing, which is not in contact with the flywheel cell spindle and is frictionless. When the flywheel battery is in working condition and the magnetic suspension bearing fails or the main shaft of the flywheel battery is subjected to a large impact and the magnetic suspension bearing is not effectively adjusted, the auxiliary bearing assumes the role of accepting the impact of the main shaft of the flywheel battery and bears part or all of the load to protect the magnetic suspension bearing from being damaged by the impact. Considering that the flywheel battery spindle may be subjected to both radial and axial impact, the auxiliary bearing needs to bear both radial and axial loads, so the auxiliary bearing in this paper selects the form of angular contact bearing or a combination of deep groove ball bearing and angular contact bearing.

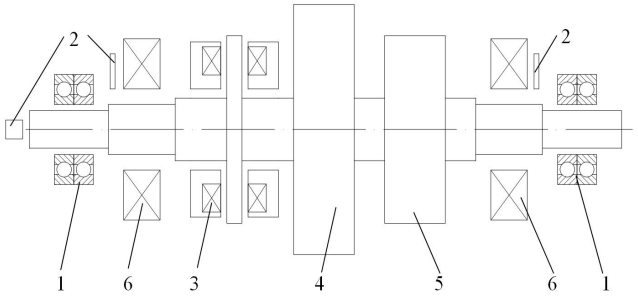

1.Mechanical Bearing 2.Eddy current displacement sensor 3.Axial magnetic bearing 4.Flywheel rotor 5.Motor rotor 6.Radial magnetic bearing

Fig. 2 Flywheel battery support topology scheme

III. RADIAL ELECTROMAGNETIC BEARING STRUCTURE DESIGN

A. Radial magnetic bearing rotor design

The rotor and stator of the radial magnetic levitation bearing form a magnetic circuit, which allows the stator electromagnetic force to drive the flywheel battery spindle and maintain a stable levitation task. The rotor material needs to have a high relative permeability, saturation magnetic density, and good demagnetization characteristics, which also considering eddy current losses. Therefore, this design uses a laminated silicon steel material and a sleeve-type structure, which is fixed to the flywheel cell spindle by interference fit to avoid loosening during normal operation. The inner diameter size of the rotor can be determined based on the main shaft of the flywheel cell. The yoke width is not smaller than the stator pole width to reduce the occurrence of magnetic leakage.

$$D = d + 2e \tag{1}$$

where D is the rotor outer diameter, d is the rotor inner diameter, and e is the rotor yoke width.

The design radial magnetic levitation bearing rotor axial length is slightly larger than the radial levitation magnetic bearing stator axial length. As follows:

$$L_1 = L + \Delta l \tag{2}$$

where L_1 is the rotor width.

B. Radial magnetic levitation bearing stator design

The basic structure of the designed radial magnetic levitation bearing is shown in Fig. 3. The design of the stator in a radial magnetic levitation bearing primarily includes the design of magnetic poles, the design of the magnetic yoke, and the structural design of the coil slot and other components. In Fig. 3, D is the rotor outer diameter, D_1 is the stator inner diameter, D_2 is the stator middle diameter, D_3 is the stator outer diameter, P is the pole width, H is the coil winding length, C is the one-sided air gap value, and L is the magnetic levitation bearing width.

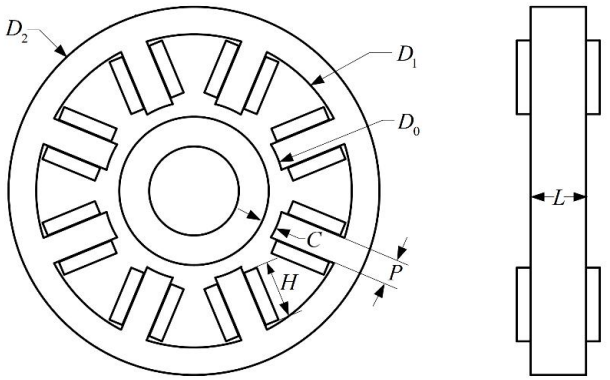

Fig. 3 The structure of the radial magnetic bearing

The inner diameter of the stator is determined based on the outer diameter of the rotor and the value of the air gap. Where the air gap value between stator and rotor is based on the rotor outer diameter for design.

$$D_1 = D + 2c \tag{3}$$

The pole width is determined by the inner diameter of the stator and the number of poles. In this paper, the pole width P is defined as the width of the stator slot, allowing sufficient clearance for the installation of the coil winding and utilization of the pole area.

$$P = \frac{\pi D_2}{2N_p} \tag{4}$$

The yoke width C is designed to be no less than the pole width to reduce the magnetic leakage of the radial magnetic levitation bearing at the yoke.

$$C = (1 \sim 1.5) \times P \tag{5}$$

From the simplified mechanical model of magnetic levitation bearing, we calculate the maximum load capacity that can be provided by a single magnetic pole.

Due to the combined effect of the upper and lower magnetic poles in the radial magnetic levitation bearing, the maximum load capacity of the bearing can be determined.

$$F_s = \frac{B_{max}^2 A}{2\mu_0} \tag{6}$$

$$F_{max} = 2F_s \cos\alpha = \frac{B_{max}^2 A}{\mu_0}\cos\alpha \tag{7}$$

where F_{max} represents the maximum bearing load capacity, and F_s denotes the load capacity of a single magnetic pole.

Based on the maximum load carrying capacity of the radial magnetic levitation bearing, the magnetic pole area A of a single pole can be further deduced.

$$A = \frac{\mu_0 F_{max}}{B_{max}^2 \cos\alpha} \tag{8}$$

Further, the axial length L and width of the magnetic levitation bearing can be calculated using the magnetic pole area and the magnetic pole width.

$$L = \frac{F_s u_0}{B_{max}^2 P \cos\alpha} = \frac{2N_p F_s u_0}{\pi D_1 B_{max}^2 \cos\alpha} \tag{9}$$

When the current in the coil winding reaches its maximum design level, the magnetic flux circuit achieves its highest magnetic induction strength. The number of turns in the coil winding can be calculated using the simplified mechanical model of magnetic levitation bearing.

$$N_{all} I_{max} = \frac{2B_{max} c}{\mu_0} \tag{10}$$

With the maximum design current of the coil winding as the maximum allowable current, the minimum wire diameter dc of the coil winding wire can be calculated.

$$d_c = \sqrt{\frac{4I_{max}}{\pi J}} \tag{11}$$

where J is the maximum permissible current density of the wire material, which is related to the wire material and the insulation level and cooling conditions of the coil winding.

In the area of the stator coil cavity A_{cu}, the stator window depth H can be deduced.

$$A_{cu} = \frac{1}{2N_p} H\left[\frac{\pi}{2}D_2 + \pi(D_2 + H) - \frac{\pi}{2}D_2\right] = \frac{\pi(D_2 + H)}{2N_p} H \tag{12}$$

$$H = \frac{\sqrt{D_2^2 + 8N_p \frac{A_{cu}}{\pi}} - D_2}{2} n \tag{13}$$

IV. Axial Electromagnetic Bearing Structure Design

The basic structure of the designed axial magnetic levitation bearing is shown in Fig. 4. In Fig. 4, the following dimensions are labeled: d for the spindle outer diameter, d_1 for the inner ring inner diameter, d_2 for the inner ring outer diameter, d_3 for the outer ring inner diameter, d_4 for the outer ring outer diameter, h for the yoke width, c for the one-sided air gap value, d_5 for the thrust disc outer diameter, and L for the thrust disc thickness.

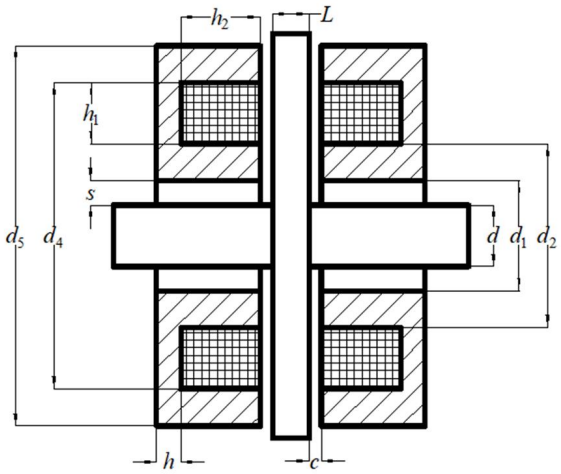

Fig. 4 Axial magnetic bearing construction diagram

A. Design of axial magnetic levitation bearing stator structure

In the structural design of the axial magnetic bearing, the principle of equal magnetoresistance is utilized to ensure that the magnetic induction intensity in the magnetic flux circuit of both the inner and outer rings of the axial magnetic bearing is equal.This allows for the optimal utilization of the stator material. According to the equal area magnetic loop method, the inner and outer rings (A_{in}, A_{out}) of axial magnetic bearings have equal magnetic pole areas A_0.

$$A_{in} = A_{out} = A_0 \tag{14}$$

Combined with the maximum load carrying capacity of axial magnetic bearing design, the magnetic pole area can be calculated using the simplified mechanical model of magnetic bearing.

$$A_0 = \frac{\pi\left(d_2^2 - d_1^2\right)}{4} = \frac{\pi\left(d_4^2 - d_3^2\right)}{4} = \frac{\mu_0 F_d}{B_0^2} \tag{15}$$

The air gap value of the axial magnetic levitation bearing is determined based on the diameter of the rotor. Based on the diameter of the flywheel cell spindle, the air gap value of the axial magnetic bearing on one side is determined to be 0.3mm. Meanwhile, the spacing between the stator and rotor of an axial magnetic bearing is determined based on the axial air gap and in accordance with the empirical formula.

$$s = (3 \sim 10)c \tag{16}$$

After the spacing between the bearing magnetic bearing and the spindle is determined, the inner diameter and outer diameter of the stator inner ring of the axial magnetic levitation bearing are obtained.

$$d_1 = d_0 + s \tag{17}$$

$$d_2 = \sqrt{\frac{4A_0}{\pi} + d_1^2} \tag{18}$$

With the maximum design current of the coil winding set as the maximum allowable current, the minimum diameter of the coil winding wire is calculated.

$$d_c = \sqrt{\frac{4I_{max}}{\pi J}} \tag{19}$$

Based on the coil slot area, calculate the width and height of the coil slot.

$$h_1 = h_2 = \sqrt{A_w} \tag{20}$$

Based on the outer diameter of the inner ring of the stator and the height of the coil slot, the inner and outer diameters of the outer ring of the stator for the axial magnetic bearing are determined.

$$d_3 = d_2 + 2h \tag{21}$$

Axial magnetic levitation bearing stator outer ring outer diameter: from the formula, according to the outer ring pole area and the stator outer ring inner diameter to calculate the stator outer ring outer diameter.

$$d_4 = \sqrt{\frac{4A_0}{\pi} + d_3^2} \tag{22}$$

At the same time, in order to minimize magnetic leakage, it is necessary for the area of the stator yoke of the axial magnetic bearing to be equal to or larger than the area of the magnetic pole. As follows:

$$\pi d_2 h \geq A_0 \tag{23}$$

B. Design of axial magnetic levitation bearing thrust disc structure

The thrust disk, also known as the axial magnetic levitation bearing rotor, is made of a single piece of ferromagnetic material. The main structural parameters of the disk are its outer diameter and thickness. To minimize magnetic leakage, the outer diameter of the thrust disk is slightly larger than that of the stator in the axial magnetic levitation bearing.

$$d_5 = d_4 + (1 \sim 2) \tag{24}$$

The thickness of the axial magnetic levitation bearing yoke is chosen to be equal to or greater than the thickness of the thrust disc.

$$L > h \tag{25}$$

V. Control Strategy Design

From the simplified mechanical model of the magnetic levitation bearing, a Taylor expansion is performed on the electromagnetic combined force acting on the rotor to obtain the force-displacement function.

$$\begin{cases} F = k_i i + k_x x \\ k_i = \dfrac{\mu_0 N^2 A I_0}{2x^2} \\ k_x = \dfrac{\mu_0 N^2 A I_0^2}{2x^3} \end{cases} \tag{26}$$

where k_i represents the current stiffness coefficient of the magnetic levitation bearing, and k_x represents the displacement stiffness coefficient of the magnetic levitation

bearing.

Fig. 5 shows the schematic diagram of the closed-loop differential control of the magnetic levitation bearing [24]. In the vertical direction, the rotor of the magnetically levitated bearing is subjected to the combined action of electromagnetic force and gravity. According to Newton's second law, the equation of motion for the rotor is obtained as:

$$m\ddot{x} = F - mg \tag{27}$$

$$m\ddot{x} = k_i i + k_x x - mg \tag{28}$$

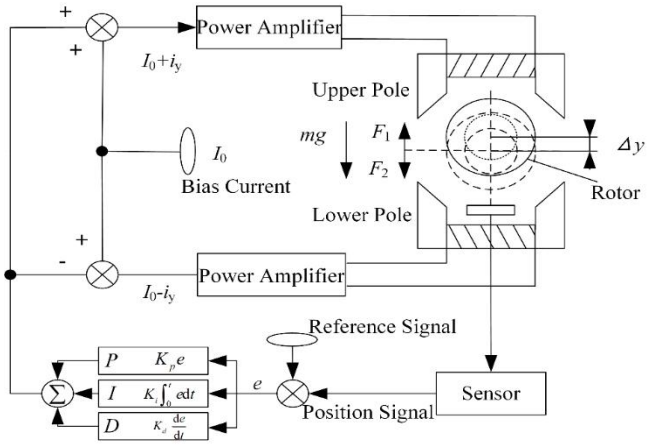

Fig. 5 Diagram of the closed-loop differential control structure for magnetic bearings

Laplace transformation is performed to obtain the transfer function for a single degree of freedom in a magnetically levitated bearing. The input is the current and the output is the displacement. The process is as follows:

$$G(s) = \frac{X(s)}{I(s)} = \frac{k_i}{ms^2 - k_x} \tag{29}$$

The equation shows that there are two poles of the controlled object, located on the positive and negative real axes of the complex plane. According to control theory, the controlled object is an unstable second-order object. To eliminate the instability of the system and achieve stable suspension of the rotor at the working point position, it is necessary to add a closed-loop control link. Using the current control scheme, the transfer function for PID control can be derived.

$$G_c(s) = K_p + \frac{K_d s}{1 + T_d s} + \frac{K_i}{s} \tag{30}$$

Power amplifiers play a crucial role in signal amplification, and voltage-current power amplifiers are commonly utilized. In this paper, we introduce a hysteresis link to simulate the transfer function of the voltage-current power amplifier.

$$G_a(s) = \frac{A_a}{1 + T_a s} \tag{31}$$

where A_a is the amplification coefficient of the power amplifier, and T_a is the hysteresis coefficient of the power amplifier. In practical applications, the hysteresis coefficient of the power amplifier is typically very small and can generally be disregarded.

Displacement sensors mostly use an eddy current displacement sensor, which converts the distance between the eddy current probe coil and the measured metal body into electrical parameters such as equivalent inductance, equivalent impedance, and quality factor of the coil, which is converted into a voltage signal by the preamplifier in to realize the measurement of displacement. In the feedback loop of the magnetic levitation bearing system, the hysteresis loop is added to simulate the transfer function of the eddy current displacement sensor.

$$G_s(s) = \frac{A_s}{1 + T_s s} \tag{32}$$

where A_s is the amplification coefficient of the displacement sensor, T_s is the hysteresis coefficient of the displacement sensor. In practical applications, the hysteresis coefficient of the displacement sensor is typically very small and can generally be disregarded.

According to the above, the complete transfer function of the control system can finally be derived.

$$G(s) = \frac{\left(\frac{A_a}{1+T_a s}\right)\left(K_p + \frac{K_d s}{1+T_d s} + \frac{K_i}{s}\right)\left(\frac{K_{ix}}{ms^2 - K_{xx}}\right)}{1 + \left(K_p + \frac{K_d s}{1+T_d s} + \frac{K_i}{s}\right)\left(\frac{A_a}{1+T_a s}\right)\left(\frac{A_s}{1+T_s s}\right)\left(\frac{K_{ix}}{ms^2 - K_{xx}}\right)} \tag{33}$$

VI. Performance Analysis

A. Analysis of magnetic induction strength of axial magnetic levitation bearings

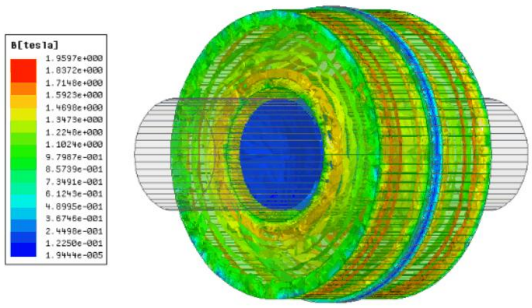

(a) Cloud map of magnetic induction intensity

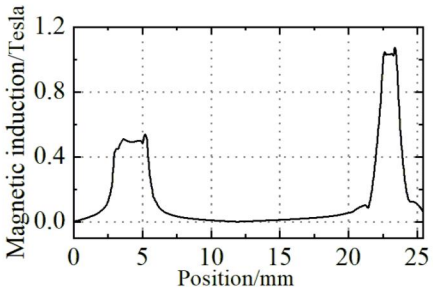

(b) Magnetic induction at the air gap

Fig. 6 Magnetic induction intensity of the axial magnetic bearing

As shown in Fig. 6(a), the magnetic lines and magnetic induction intensity distribution of the axial magnetic levitation bearing are displayed. The magnetic lines are

concentrated around the coil winding, and there is a certain amount of leakage at the top of the thrust disk and the gap between the axial magnetic levitation bearing and the main shaft. As a whole, most of the magnetic lines form a magnetic flux circuit through the inner ring of the stator, the outer ring of the stator, the thrust disk, and the bearing gap of the axial magnetic bearing, and there is only a magnetic leakage at the gap with the main shaft. Fig. 6(b) shows the curve depicting the change in magnetic induction intensity at the air gap of an axial magnetic levitation bearing. The magnetic induction intensity at the air gap of the axial magnetic levitation bearing is 1.07T, which is very close to the design value of 1.1T and meets the design requirements.

B. Analysis of the influence of the excitation method on the magnetic circuit distribution and magnetic pole coupling in radial magnetic levitation bearings

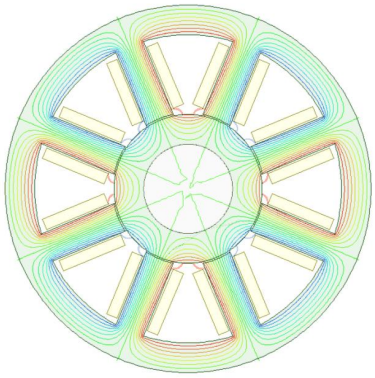

(a) NSNS type topology magnet line distribution

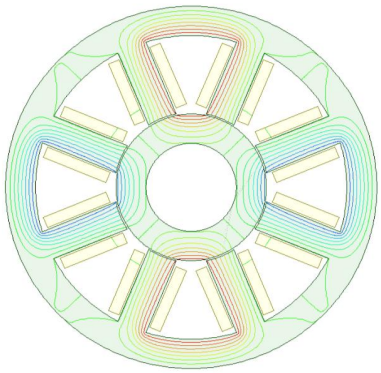

(b) NNSS type topology magnet line distribution

Fig. 7 NSNS/NNSS type topology magnet line distribution

When all poles of an 8-pole radial magnetic bearing are conducting bias current, it is similar to a magnetic bearing in normal operation. For the 8-pole radial magnetic bearing, the most commonly used pole topologies are NSNS type, NNSS type, NNNN type, and SSSS type. Fig. 7(a) shows the distribution of magnetic force lines for the NSNS type topology. As can be seen from Fig. 7(a), in this topology, the magnetic lines of force permeate the entire stator and rotor of the magnetic bearing, and the interaction between the magnetic poles is significant. There is a strong coupling between the adjacent poles, and the magnetic lines of force pass through the end surfaces of the stator poles to form a circuit with the two adjacent poles. However, there is a small amount of magnetic leakage at the air gap. Under this topology, the direction of the electromagnetic force formed by each pole is angled both horizontally and vertically. This adversely affects the stability and control of the magnetically levitated bearing rotor.

Fig. 7(b) shows distribution of magnetic force lines for the NNSS type topology. As can be seen from the Fig. 7(b), in this topology, the magnetic force lines form a closed loop between two poles of opposite polarity. Compared to the NSNS type topology, the coupling of the NNSS type topology is significantly enhanced, resulting in improved magnetic leakage and concentrated distribution of magnetic force lines. This makes it easier to achieve control over electromagnetic force.

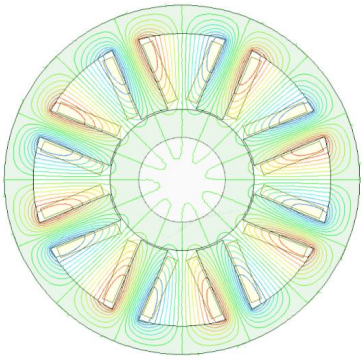

(a)NNNN type topology magnet line distribution

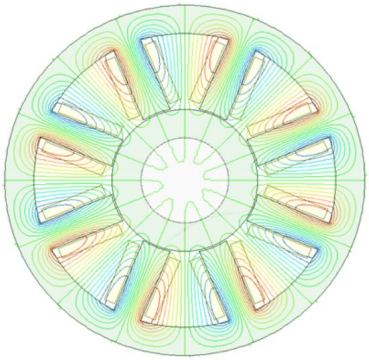

(b) SSSS type topology magnet line distribution

Fig. 8 NNNN/SSSS type topology magnet line distribution

Fig. 8 shows the distribution of magnetic lines between NNNN type and SSSS type topology. The NNNN type topology is similar in principle to the SSSS type topology. It can be seen from Fig. 8 that there is almost no coupling between the magnetic poles of these two topologies, which is much better than the NSNS type topology and the NNSS type topology. However, in the NNNN type and the SSSS type, a significant amount of magnetic flux lines form loops directly in the air, leading to substantial magnetic leakage. The magnetic flux density throughout the entire structure is very low and cannot effectively generate electromagnetic force. The NNSS topology is the most suitable configuration for the 8-pole radial magnetic levitation bearing. On the whole, this topology exhibits good magnetic pole coupling, low magnetic flux interference between different poles, and can effectively provide electromagnetic force. This reduces the design complexity for the controller and meets the support requirements of the magnetic levitation bearing.

C. Analysis of bearing dynamic response performance

The tested magnetic levitation bearing prototype is shown in Fig. 9. A controller based on the integrated design of the digital signal processor TMS320C28346 with a main

frequency of 300 MHz is applied, and its chip integrates an abundance of peripheral resources. In this setup, the current sensor is integrated into the hardware controller, and it has an accuracy of ±0.5%. The displacement data is obtained by an ML33 eddy current displacement transducer with an accuracy of 0.1 μm.

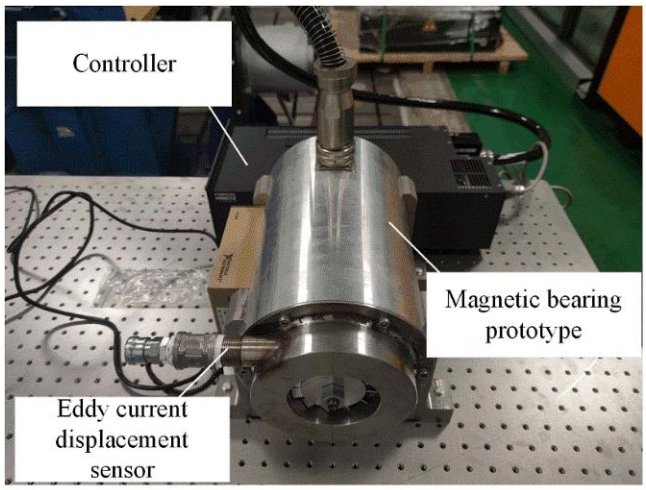

Fig. 9 Magnetic levitation bearing test prototype

The Simulink model is built and automatically compiled in the rapid prototyping system. Subsequently, it is downloaded to the integrated controller to implement the control test of the maglev bearing. The NNSS topology was selected, and a prototype radial magnetic levitation bearing was developed. In the experiment, the gain of the eddy current displacement sensor is 0.4 A/V, and the gain of the power amplifier is 5×10^3 V/m. The gain of the A/D converter and D/A converter are 819 V^{-1} and 1.22×10^{-3} V, respectively. The mass of the magnetic levitation bearing rotor is 6.5×10^{-2} kg, and the current stiffness factor and displacement stiffness factor are 49 N/m and 61250 N/m, respectively.

The schematic diagram of the levitation-bearing control system is shown in Fig. 10. It mainly consists of the controller, power amplifier, displacement sensor, A/D converter, D/A converter, and magnetic levitation bearing stator and rotor components. The displacement is determined using an eddy current displacement sensor. This sensor converts the distance between the coil of the eddy current probe and the metal body being tested into electrical parameters, such as equivalent inductance, equivalent impedance, and quality factor of the coil. Eventually, it is converted into a voltage signal for measuring displacement. The current signal originates from the control signal and is amplified by the controller and power amplifier. It is then transmitted to the stator coil of the magnetic levitation bearing, which ultimately controls the rotation of the rotor.

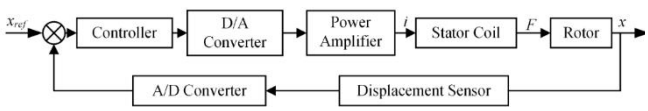

Fig. 10 Schematic diagram of the suspension bearing control system

The dynamic response of the bearing displacement and the control current variation characteristics of the magnetic bearing under step and sinusoidal excitation are given in Fig. 11 and 12, respectively. The step signal and sinusoidal period signal are applied to the controller as excitations to produce a 0.1mm offset of the magnetic levitation bearing rotor based on the starting position. From the step response results, it can be seen that the magnetic levitation bearing rotor can achieve undulation control and stabilize at 0.1mm in response to the required position signal. This meets the requirement for stable levitation at the target position. From the sinusoidal response results, it can be seen that the curve-following effect of the output displacement signal obtained by applying a sinusoidal excitation of 12.5 Hz to the target meets the required criteria.

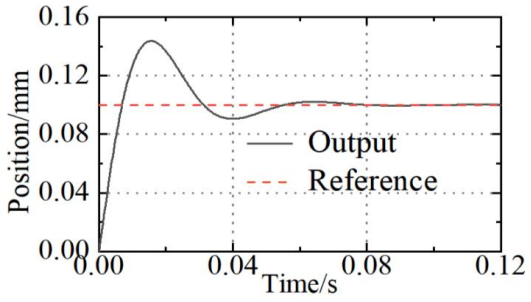

(a)Step excitation response

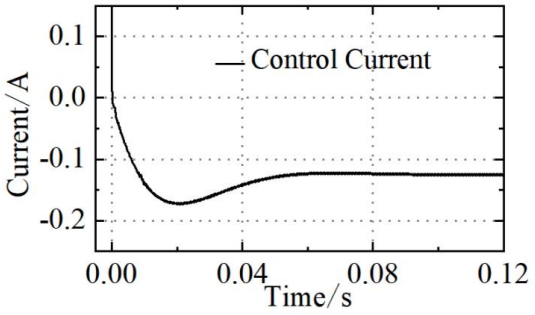

(b) Control Current of Step excitation

Fig. 11 Displacement response and control current of a magnetic bearing under step excitation

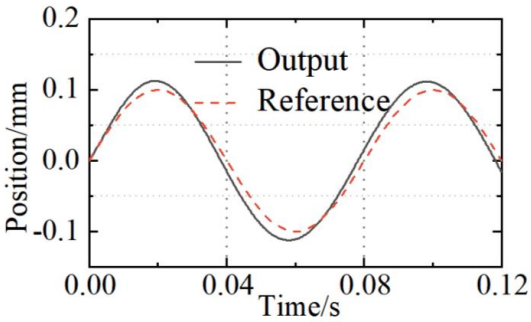

(a)Sinusoidal excitation response

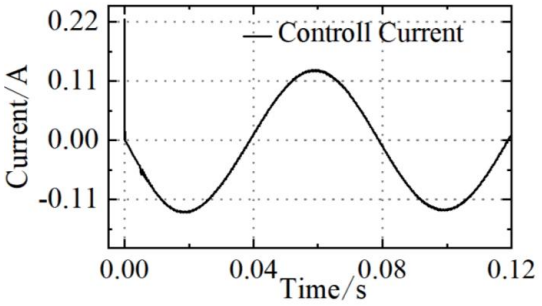

(b) Control Current of Sinusoidal excitation

Fig. 12 Displacement response and control current of a magnetic bearing under sinusoidal excitation.,

VII. Conclusions

In this paper, we study a magnetic levitation bearing for a high-speed flywheel battery for vehicles. A novel solution for supporting flywheel batteries is provided, resulting in a significant improvement in their efficiency and lifespan.

(1) The active magnetic levitation bearing is applied to the flywheel battery, and this innovative design offers a unique solution for the design of a new class of flywheel battery support systems. To ensure smooth crossing of the critical speed point by the flywheel rotor, the design of the flywheel cell support structure topology scheme should incorporate radial magnetic levitation bearings, axial magnetic levitation bearings, and mechanical bearings.

(2) A scheme for optimizing the structure of a radial magnetic levitation bearing is designed to effectively improve the load carrying capacity and alleviate the edge effect and the phenomenon of magnetic force line gathering at the magnetic pole. Compared with the bearings of NSNS type, NNNN type, and SSSS type, the pole coupling and magnetic leakage problems are solved by the NNSS type.

(3) The feasibility of the designed prototype and scheme is verified through simulation and test results. The results show that the magnetic levitation bearing can achieve the desired control objective and stabilize at a safe interval position under the influence of step and sinusoidal external excitation.

References

[1] Arani, A.K., Karami, H., Gharehpetian, G., Hejazi, M. (2017). Review of Flywheel Energy Storage Systems structures and applications in power systems and microgrids. Renewable and Sustainable Energy Reviews , 69, 9-18.

[2] Cimuca, G.O., Saudemont, C. Robyns, B. Radulescu. (2006). Control and performance evaluation of a flywheel energy-storage system associated to a variable-speed wind generator. IEEE Transactions on Industrial Electronics, 53, 1074-1085.

[3] Liu, H., Jiang, J. (2007). Flywheel energy storage—An upswing technology for energy sustainability. Energy & Buildings, 39, 599-604.

[4] Dhand, A., Pullen, K. (2013). Review of flywheel based internal combustion engine hybrid vehicles. International Journal of Automotive Technology, 14, 797-804.

[5] Hansen, J.G. An assessment of flywheel high power energy storage technology for hybrid vehicles, Oak Ridge National Lab., Oak Ridge, TN: 05 2012.

[6] Wen, Z., Fang, P., Yin, Y., Królczyk, G., Gardoni, P., Li, Z. (2022). A novel machine learning model for safety risk analysis in flywheel-battery hybrid energy storage system. Journal of Energy Storage, 49, 104072.

[7] Li, H., Chu, J., Sun, S. (2022). Development of a Flywheel Hybrid Power System in Vehicles without the Electric Drive Device Rated Capacity Limit. World Electric Vehicle Journal, 13, 27.

[8] Hasegawa, H., Matsue, H., Nagashima, K., Yamashita, T. (2016). Flywheel energy storage system using superconducting magnetic bearings for demonstration tests. Quarterly Report of RTRI, 57, 221-227.

[9] Fang, S., Lv, Z., Chao, G. (2021). Methods of increasing the energy storage density of superconducting flywheel. IEEE Transactions on Applied Superconductivity, 31, 1-5.

[10] Morehouse, D., Arnett, D., Hess, H., Berven, C. (2019). Dynamic behavior of superconductor-permanent magnet levitation with halbach arrays for flywheel design and control. IEEE Transactions on Applied Superconductivity, 29, 1-5.

[11] Choudhury, S. (2021). Flywheel energy storage systems: A critical review on technologies, applications, and future prospects. International Transactions on Electrical Energy Systems, 31, e13024.

[12] Li, X., Palazzolo, A. (2022). A review of flywheel energy storage systems: state of the art and opportunities. Journal of Energy Storage, 46, 103576.

[13] Ren, X., Feng, M., Ren, T. (2018). Design and optimization of a radial high-temperature superconducting magnetic bearing. IEEE Transactions on Applied Superconductivity, 29, 1-5.

[14] Qiu, Y., Jiang, S. (2019). Suppression of low-frequency vibration for rotor-bearing system of flywheel energy storage system. Mechanical Systems and Signal Processing, 121, 496-508.

[15] Dagnaes-Hansen, N.A., Santos, I.F. (2019). Permanent magnet thrust bearings for flywheel energy storage systems: Analytical, numerical, and experimental comparisons. Proceedings of the Institution of Mechanical Engineers, Part C: Journal of Mechanical Engineering Science, 233, 5280-5293.

[16] Zhu, H., Liu, T. (2020). Rotor displacement self-sensing modeling of six-pole radial hybrid magnetic bearing using improved particle swarm optimization support vector machine. IEEE Transactions on Power Electronics, 35, 12296-12306.

[17] Wang, H., Wu, Z., Liu, K., Wei, J., Hu, H. (2022). Modeling and Control Strategies of a Novel Axial Hybrid Magnetic Bearing for Flywheel Energy Storage System. IEEE/ASME Transactions on Mechatronics.

[18] Soni, T., Dutt, J.K., Das, A.S. (2019). Parametric stability analysis of active magnetic bearing supported rotor system with a novel control law subject to periodic base motion. IEEE Transactions on Industrial Electronics, 67, 1160-1170.

[19] Suhang, Y., Wenyong, G., Yuping, T., Wenju, S., Yang, C., Chenyu, T. (2021). A review of the structures and control strategies for flywheel bearings. Energy Storage Science and Technology, 10, 1631.

[20] Shata, A.M.A.-H., Hamdy, R.A., Abdelkhalik, A.S., El-Arabawy, I. (2018). A fractional order PID control strategy in active magnetic bearing systems. Alexandria engineering journal, 57, 3985-3993.

[21] Sun, J., Zhou, H., Ma, X., Ju, Z. (2018). Study on PID tuning strategy based on dynamic stiffness for radial active magnetic bearing. ISA transactions, 80, 458-474.

[22] Starbino, A.V., Sathiyavathi, S. (2019). Real-time implementation of SMC–PID for magnetic levitation system. Sādhanā, 44, 1-13.

[23] Dhand, A., Pullen, K. 2015). Review of battery electric vehicle propulsion systems incorporating flywheel energy storage. International Journal of Automotive Technology, 16, 487-500.

[24] P. Wang, T. Gu, B. Sun, "Control Strategy Design of Active Magnetic Levitation Bearing for High-speed Flywheel Energy Storage Device," IAENG International Journal of Applied Mathematics, vol. 52, no.4, pp910-917, 2022.